chemosensors

MDPI

Review

A Review of Nanostructured Resistive-Based Vanadium Oxide Gas Sensors

Vahid Amiri [1], Hossein Roshan [2], Ali Mirzaei [1,*] and Mohammad Hossein Sheikhi [2,*]

[1] Department of Materials Science and Engineering, Shiraz University of Technology, Shiraz 71555-13876, Iran; vamiri1365@gmail.com

[2] School of Electrical and Computer Engineering, Shiraz University, Shiraz 51154-71348, Iran; hossein.roshan@shirazu.ac.ir

* Correspondence: mirzaei@sutech.ac.ir (A.M.); msheikhi@shirazu.ac.ir (M.H.S.)

Received: 22 September 2020; Accepted: 23 October 2020; Published: 25 October 2020

Abstract: Vanadium pentoxide (V_2O_5) is a transition metal oxide with features such as high availability, good catalytic activity, unique electrical properties and high conductivity which are appropriate for gas sensing applications. In this review, we discuss different gas sensing aspects of V_2O_5 in pristine, doped, decorated and composite forms. Depending on its synthesis procedure, morphology, sensing temperature and surface conditions, the V_2O_5-based gas sensors show different responses to target gases. Herein, we have discussed the behavior of V_2O_5-based gas sensors to different gases and associated sensing mechanisms. This review paper can be a useful reference for the researchers who works in the field of gas sensors.

Keywords: V_2O_5; gas sensor; morphology; sensing mechanism; toxic gas

1. Introduction

Vanadium (V) is a well-known transition metal which can form different oxides. The principal oxides of vanadium are vanadium monoxide (VO, violet color), vanadium sesquioxide (V_2O_3, green color), vanadium dioxide (VO_2, blue color), and vanadium pentoxide (V_2O_5, yellow color). Presence of oxygen vacancies leads to formation other oxides such as V_3O_7, V_4O_9, and V_6O_{13} (a mixture of V^{5+} and V^{4+}), and a series of oxides such as V_6O_{11}, V_7O_{13}, and V_8O_{15} (a mixture of V^{4+} and V^{3+}). In general, the mixing phases can be categorized into two series of phases namely the Magnéli phase (V_nO_{2n-1}) and the Wadsley phase V_nO_{2n+1} [1,2]. Among different phases, V_2O_5 is thermodynamically the most stable oxide and it exist in different polymorphs namely the most stable α-V_2O_5 (orthorhombic), metastable β-V_2O_5 (tetragonal or monoclinic), γ-V_2O_5 (orthorhombic) and δ-V_2O_5 (monoclinic) [3]. Each polymorph is stable at a temperature and pressure range. For example, β-V_2O_5 is stable at high pressure and temperatures [4].

The orthorhombic V_2O_5 has a layered structure and it is comprised of the distorted polyhedra of six oxygen atoms which form octahedral polyhedra with central V atoms [5]. There are three different oxygen positions in the V_2O_5 crystal structure. The VO_6 octahedra are linked, sharing edges through the chain (O_c) and corners via the bridging oxygens (O_b). Two vanadyl oxygen atoms (O_v) form the vertices of the octahedra along the c-axis [6].

V_2O_5 is highly abundant in nature, it has low price and has several oxidation states [7,8]. Accordingly, due to its relatively open layered structure and its unique properties, V_2O_5 has been used in different applications such as water splitting [9], field effect transistors [10,11], supercapacitors [12], IR detectors [13], photodetectors [14], UV sensors [15], optical sensors [16], amprometric gas sensors [17], potentiometric sensors [18] electrochemical sensors [19,20], cataluminescence sensors [21], resistance gas sensors [22,23], gasochromic sensors [24] and humidity sensors [25].

V_2O_5 with an n-type semiconducting behavior, has a relatively high conductivity (0.5 $S{\cdot}cm^{-1}$) at room temperature [26]. At high temperatures, stoichiometric V_2O_5 spontaneously converts to V_2O_{5-x} as follows:

$$V_2O_5 \leftrightarrow V_2O_{5-x} + \frac{x}{2}O_2 \quad x \sim 0.01 \tag{1}$$

Values of "x" vary depending on annealing temperature and oxygen partial pressure during synthesis. As a result, oxygen vacancies form in the oxygen sub-lattice and n-type semiconducting is induced. To be neutral, some V^{5+} ions will be reduced to V^{4+} ions. Electrical conductivity in V_2O_{5-x} is due to jumping (hopping) of the electrons from V^{4+} ions to the neighboring V^{5+} ions [26].

Compared with bulk V_2O_5, nanostructured V_2O_5 materials have unique electrical and chemical properties and due to their ultrafine sizes, they offer a high surface area which is extremely beneficial for sensing studies [27–30].

Nowadays gas sensors have become widely used in different areas for detection of toxic, hazardous, explosive and greenhouse gases and vapors [31,32]. There are many types of gas sensors. However, resistive-based gas sensors using metal oxides are the most widely used gas sensors due to their unique features such as low price, high sensitivity, high stability, fast dynamics and simple fabrication and operation [33,34]. Figure 1 shows a typical gas sensor substrate, where its front side is equipped with conductive electrodes such as with Pt and its back side is equipped with a heater [35]. Herein, we comprehensively discuss different aspects of the gas sensing properties of V_2O_5-based nanomaterials. Previously, only one review paper about gas sensing properties of vanadium oxides has been published [36], and herein, we have comprehensively discussed pristine, decorated, doped and composite forms of V_2O_5 nanostructured materials with different morphologies for the gas sensing studies.

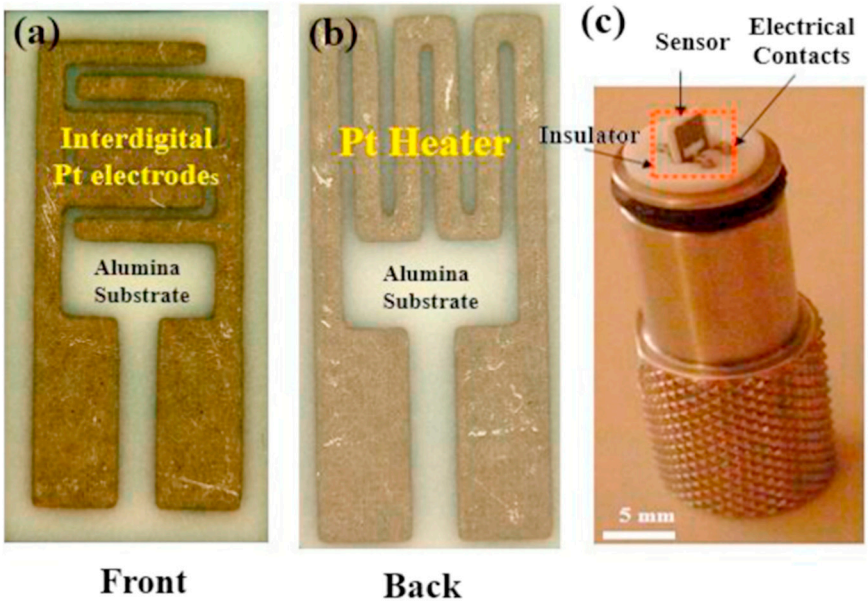

Figure 1. (**a**) Front side of substrate equipped with electrodes, (**b**) back side of substrate equipped with a heater, (**c**) sensor holder [35].

2. Pristine Nanostructured V_2O_5 Gas Sensors

Pristine V_2O_5 gas sensors with different morphologies have been reported in the literature. In this section, we discuss some of most important pristine V_2O_5 gas sensors. The gas sensing characteristics of V_2O_5 hierarchical architectures, especially for hollow spheres are rarely reported in the literature. In this regard, V_2O_5 hollow spheres (500–550 nm in diameter and a shell thickness of 55 nm) were synthesized through a solvothermal route. The hollow spheres were comprised of nanoplates with thicknesses of 50–80 nm and lengths of 70–120 nm. Moreover, for comparison solid nanostructured

spheres were fabricated. The maximum responses (R_a/R_g) to trimethylamine (TEA) at 370 °C were 9.7 for V_2O_5 hollow spheres and 3.08 for V_2O_5 solid spheres, respectively. In fact, the hollow sphere hierarchical architecture with a higher surface area offered more adsorption sites for TEA molecules and a higher response for hollow spheres resulted. The sensing mechanism of the sensor to TEA was related to the reduction of V^{5+} ions to V^{4+} ions in the presence of TEA. Furthermore, based on XPS studies there was a slight shift to lower binding energy values after exposure of the sensor to TEA gas, confirming formation of V^{4+} ions. In addition, a color change from yellow to dark blue was observed, further confirming the formation of V^{4+} ions. V_2O_5 is an acidic oxide, which is highly suitable for the adsorption of basic molecules, such as TEA and consequently a larger response of the V_2O_5 hollow spheres sensor to TEA resulted [37].

Generally, resistive based gas sensors work at high temperatures, which need external heaters and increase the power consumption. Therefore, development of room temperature gas sensors not only solves above problems, but also integration with flexible substrates become easier. Furthermore, possible risk of explosion during sensing of explosive gases such as H_2 gas significantly decreases. Hollow spheres comprising numerous nanocrystals of V_2O_5 as a shell were synthesized by a facile polyol approach for room temperature hydrogen gas sensing. The surface area of hollow spheres was about 356 m^2/g and, therefore, it provided a large active surface area for adsorption of target gases. Furthermore, its porous structure led to further enhancement of gas reactions. Furthermore, the sharp corners as well as the edges of the tiny building blocks of hollow spheres were reported as highly active sites for enhancement of the sensing reactions during hydrogen sensing [38].

Another room temperature gas sensor was realized from V_2O_5 nanoneedles which were synthesized by a physical vapor deposition method [39]. The sensor exhibited a response (R_a/R_g) of 2.37 to 140 ppm acetone at room temperature. The relevant reaction was as follows:

$$(CH_3)_2CO + 4\,O_2^- \rightarrow 3CO_2 + 3H_2O + 4e^- \quad (2)$$

The most energetically favorable gas reaction is that a surface oxygen atom attacks the carbonyl carbon to form a C-O bond. Acetone contains the carbonyl group and because of the greater electronegativity of oxygen; a carbonyl group is a polar functional group and, therefore, it has a larger dipole moment (D = 2.88), relative to other tested gases, leading to the higher response of the gas sensor to acetone.

Trimethylamine (TMA; $(CH_3)_3N$)) is generated from dead fish and, therefore, the concentration of TMA is an indicator of the freshness of fish [40]. Furthermore, exposure to TMA vapor can cause nausea, headaches, and irritation to the eyes [41]. In this regard, spherical V_2O_5 hierarchical nanostructures comprised of plenty of nanosheets were produced through a hydrothermal method. The optimal sensor based on spherical V_2O_5 hierarchical nanostructures displayed a response of ~2.8 to 100 ppm TMA along with fast response/recovery times (5/28 s) at 240 °C. The spherical V_2O_5 nanostructures were comprised of numerous monocrystalline nanosheets, and therefore they have a unique three-dimensional hierarchical structure which provided plenty of active sites for gas molecules. Accordingly, the reaction between chemisorbed oxygen ions and TMA molecules, resulted in a decrease in electrical resistance and contributed to the sensor signal.

$$2(CH_3)_3N + 21O^-(ads) \rightarrow N_2 + 6CO_2 + 9H_2O + 21e^- \quad (3)$$

In addition, in a monocrystalline structure free electrons were able to transfer faster than in a polycrystalline structure, which results in fast response and recovery times of gas sensors and improvement of sensing properties [42].

In another study related to TMA detection, Meng et al. [43] reported the synthesis of V_2O_5 flower-like structures assembled by thin nanosheets by the hydrothermal process for TMA sensing researchers. Optimal gas sensors exhibited a response (R_a/R_g) of 2.2 to 5 ppm TMA at 200 °C with

long-term stability and good selectivity. The good selectivity was related to the low C—N bond energy and high electron cloud density around N atoms in TMA.

One-dimensional V_2O_5 nanostructures such as nanorods (NRs) are also very popular for gas sensing purposes [44]. In an effort by Raj et al. [45], V_2O_5 NRs with diameters in the range of 100–200 nm were synthesized using a solvothermal method. The gas sensor was fabricated in a pelletized form of V_2O_5 NRs and it showed higher response (R_a/R_g) to 5 ppm ethanol (1.04) relative to 5 ppm ammonia (1.02). However, not only were the response values low, but also the sensor did not show selectivity to ethanol gas. This can be due to the low surface area of gas sensor, resulting from the dense pellet form of the gas sensor which limited available adsorption sites for the target gas molecules. In another similar study using a pellet form of V_2O_5 nanostructures, Raj et al. [46] synthesized V_2O_5 nanostructures with nanopetal morphology via a co-precipitation method. The sensor showed very poor selectivity, and its response to ammonia and ethanol was almost the same.

1-butylamine is extensively used in many industrial fields. However, it is toxic and harmful for human health and the environment. Moreover, it is not only toxic for human beings, but also is flammable and corrosive [47]. In another study regarding 1-D materials, the role of bottom and top electrodes on the gas response of V_2O_5 nanofibers (NFs) to 1-buthylamine was investigated [48]. Both bottom electrodes (Type I), or top electrodes (Types II and III) were used. In Type I, interdigitated Au electrodes were applied. Moreover, interdigitated gold electrodes in Type II and III had different gap sizes of 5 nm and 150 nm, respectively. The target gas can be adsorbed as follows (i) intercalation adsorption into the layered structure of the fibers or adsorption on their surface, (ii) adsorption between the inter-fiber contacts, and (iii) adsorption between the fibers and the electrode surface. Only the sensor with bottom electrodes had all three adsorption sites and, accordingly, its response was higher relative to other gas sensors.

In another study related to detection of 1-buthylamine, hierarchical nanosheet-assembled V_2O_5 microflowers were hydrothermally synthesized. The gas sensor showed a higher response (~3 times) to 1- butylamine than the commercial V_2O_5 particles at 300 °C. The higher response of the flower-like V_2O_5 particles was related to the higher surface area and the unique structure of synthesized particles. The high selectivity of the V_2O_5 microflower sensor to 1-butylamime was related to the selective oxidation of 1-butylamine on the surface of V_2O_5. In fact, selective oxidation of primary amines is possible in the presence of vanadic acids. The V_2O_5 particles showed vanadic acids-like behavior due to interaction between the water molecules on the surface of the sensor, and ultimately this led to better selective oxidation of 1-butylamine, resulting in a higher response to 1- buthylamine than other tested gases [49].

Yang et al. synthesized flower-like hierarchical V_2O_5 nanostructures by a hydrothermal method (Figure 2a–d) for 1-butylamine sensing applications [47]. At 140 °C, the sensor showed a response (R_a/R_g) of 2.6 to 100 ppm 1-buthylamine with a fast response time of 6 s. On the one hand, the peculiar morphology of the sensing layer with an open structure and high surface area facilitated the adsorption and diffusion of the oxygen and 1-buthylamine. On the other hand, the intercalation of ammonium ions into the layered structures of V_2O_5 affected the sensing response, where the distances between the layers were changed upon ammonia intercalation, contributing to the resistance change of the gas sensor [47].

The effect of the crystallization temperature on the gas response of V_2O_5 NFs was investigated by Modaferri et al. [50]. They successfully prepared V_2O_5 NFs using an electrospinning technique. The samples were crystallized at 300, 400 and 500 °C. The sensor crystallized at 400 °C showed the highest response to ammonia gas at 250 °C. The improved sensing response was related to the more porous structure of this sensor. With increasing sensor porosity, more adsorption sites can be provided for the NH_3 molecules. Furthermore, gas molecules can effectively diffuse into the deeper parts of the gas sensor and increases the reactions with already adsorbed oxygen species. Overall, a higher response is expected for more porous structures.

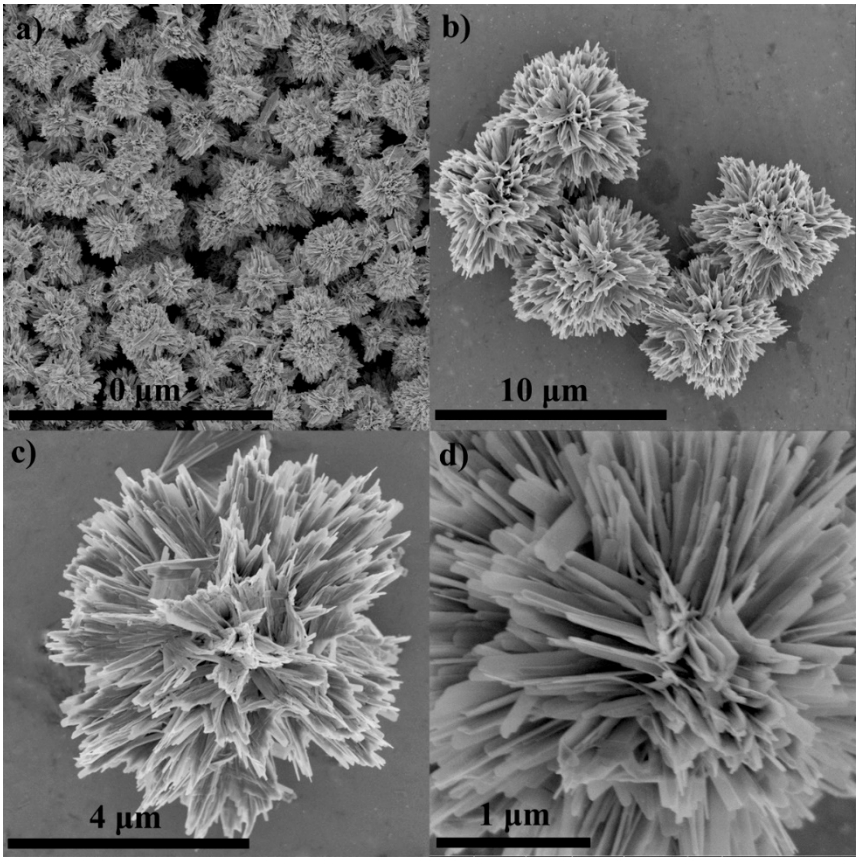

Figure 2. (**a**,**b**) low magnification; (**c**,**d**) high magnification FE-SEM images of the flower-like V_2O_5 hierarchical nano structures [47].

Methane (CH_4) is one of the greenhouse gases which is much more effective at heat trapping in the atmosphere than CO_2. Furthermore, the leakage of methane from pipelines is highly dangerous for human beings Therefore, the detection of CH_4 is important from different aspects [51]. The morphology dependence of V_2O_5 to methane gas was investigated for V_2O_5 nanostructures. Using a magnetron sputtering technique and under different sputtering powers of 100, 125 and 150 W, V_2O_5 nanostructures were synthesized with three different morphologies, where the morphology of films deposited at 100 W was NR, 125 was nanourchin and 150 W was nanoflower [52]. The resistance of NRs, nano-urchins and nanoflowers were ~15.4, 8.8 and 1.8 MΩ at room temperature (24 °C) as shown in Figure 3a. The nanoflower sensor revealed a higher sensor response among all the gas sensors at 100 °C. The nanoflower sensor displayed a higher sensing response ($\Delta R/R_a$) of 11.2% than NRs and the nano-urchin which had sensing responses of about 8.9 and 9.1% to 500 ppm CH_4 (Figure 3b–d). Enhanced response was related to the morphology of nanoflowers which were comprised of nanosheets as building blocks that eventually provided more active sites for CH_4. Furthermore, they had some voids which led to faster transfer of gases and gas sensing reactions. However, both NRs and nano-urchins had dense structures, limiting their adsorption sites as well as effective diffusion of gases to the depth parts of sensors. The good selectivity to CH_4 relative to H_2 gas was due to the difference in bond dissociation energies of C–H (413 kJ/mol) and H–H (432 kJ/mol). Owing to weaker bond dissociation energy of C–H than H–H, the reaction between C–H and V_2O_5 was easier and hence the sensor response was higher to CH_4 gas relative to H_2 gas.

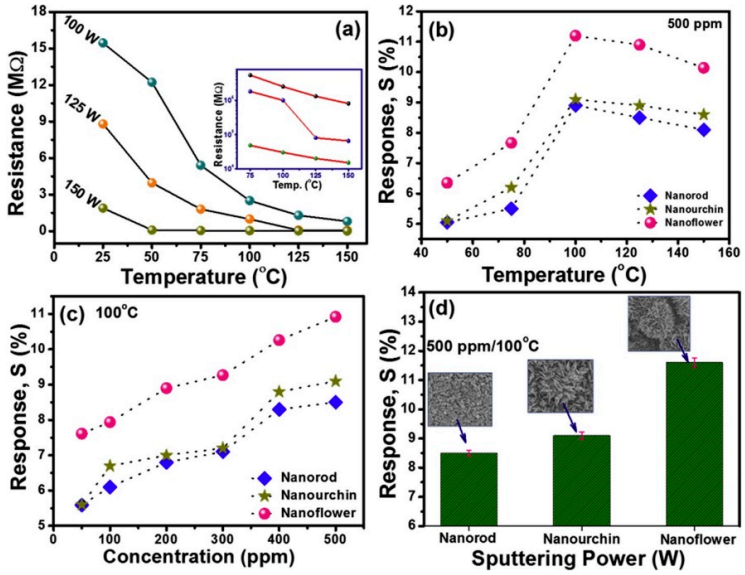

Figure 3. (**a**) Resistance versus temperature for V_2O_5 prepared under different sputtering powers (**b**) response of different morphologies of V_2O_5 as a function of temperature (**c**) response of different V_2O_5 nanostructures versus CH_4 concentrations at 100 °C. (**d**) Comparison between the response to 500 ppm CH_4 of different morphologies of V_2O_5 at 100 °C [52].

Xylene is a colorless and toxic gas which is widely used in industry mostly as solvent. However, exposure to high concentrations of xylene is dangerous for human beings and, therefore, maximum allowed exposure to xylene is set to 100 ppm for 8 h [53]. Cao et al. fabricated flower-like V_2O_5 nanostructures via hydrothermal method for gas sensing studies (Figure 4) [54]. The optimized sensor exhibited a response of 2.3 to 100 ppm xylene at 300 °C. In addition, the response time and recovery time were 44 and 78 s, respectively. Flower-like V_2O_5 with mesoporous morphology, was contained in nanoneedles, which provided a high surface area and numerous pathways to xylene gas molecules. However, its selectivity was not excellent, as its response to xylene was less than two times that of the response to buthylamine.

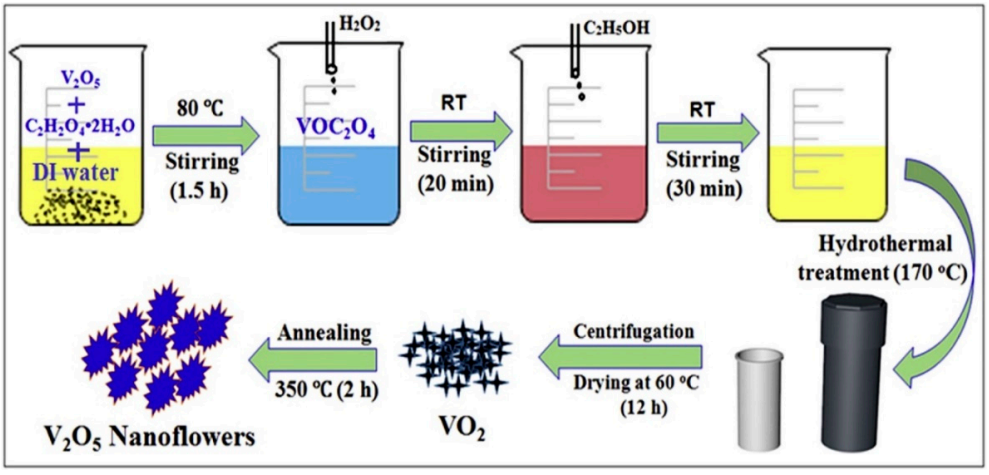

Figure 4. Schematic of preparation of flower-like V_2O_5 via hydrothermal method [54].

Helium (He) is a non-flammable gas and the second lightest element on earth, hence it is used in aero structures. Since it is an inert gas, its detection is extremely difficult with common gas sensors [55]. However, He has a relatively low atomic mass and small size, which greatly facilitates its diffusion

along the sensing layer. In an interesting study, a He gas sensor was introduced by Chauhan et al. [55]. They synthesized $V_2O_5 \cdot 1.6H_2O$ nanowires(NWs) and $V_2O_5 \cdot 1.6H_2O$ nanostars with BET surface areas of 3.58 m^2/g and 8.38 m^2/g, respectively. In fact, nanostar shapes consisted of sharp edges and therefore offered a higher surface area and a higher response, while NWs were stacked together, limiting the gas diffusion and exhibiting a lower response. Hydrated V_2O_5 contained both vanadium ions (V^{4+} and V^{5+}) which act as hopping sites for Polaron. The interaction of helium molecules with the $V_2O_5 \cdot 1.6H_2O$ nanostructures decreased the average hopping distance, resulting in an increase in the conductivity of the sensing layer. The hopping distance decreased due to an increase in hopping sites in the presence of He gas. This was due to the fact that the He gas molecule itself acted as a hopping site for charge transfer (Figure 5).

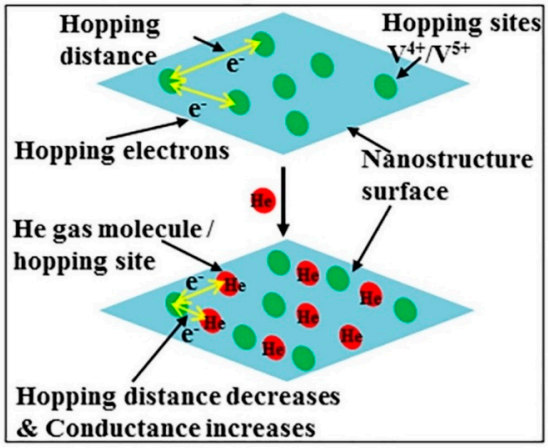

Figure 5. Sensing mechanism of hydrated V_2O_5 gas sensor to He gas [55].

Spray pyrolysis is a simple and inexpensive deposition technique which is able to deposit a large surface area with good uniformity. The effect of substrate temperature on the final sensing performance of V_2O_5 films to NO_2 gas deposited by the spay pyrolysis technique was investigated [2]. The prepared solutions were sprayed onto the glass substrate at different substrate temperatures of 350, 400, 450 and 500 °C (Figure 6). Gas sensing studies showed that the V_2O_5 thin film sensor deposited at 400 °C had the highest response to NO_2 gas at 200 °C.

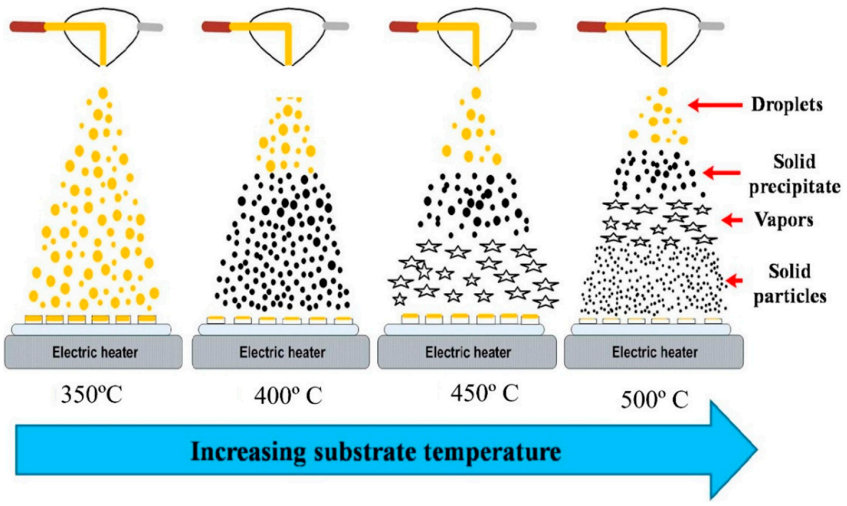

Figure 6. Deposition of V_2O_5 thin films at different substrate temperatures [2].

At high substrate temperatures, the formation of reduced V_2O_{5-x} species led to formation of oxygen vacancies. These oxygen vacancies enhanced adsorption of NO_2 gas molecules on the sensing layer. However, for the samples deposited at higher temperature, even though it was expected that more oxygen vacancies be produced, particle sizes also were larger. Therefore, the sample deposited at 400 °C, showed the optimal values of oxygen vacancies along with high surface area, which finally resulted in the best sensing response to NO_2 gas.

In another similar study, the V_2O_5 NRs were spray deposited onto the glass substrates at 400 °C using VCl_3 solutions with different concentrations of 10 to 40 mM. The V_2O_5 NRs deposited with 30 mM solution exhibited the highest gas response of 24.2% to 100 ppm NO_2 gas at 200 °C with response and recovery times of 13 s and 140 s, respectively. The improved sensing response of the optimized gas sensor was attributed to high crystallinity of sensing layer and the formation of a porous structure in which diffusion of gas molecules was facilitated into the depth parts of gas sensor [56].

In another study related to spray pyrolysis deposition technique, nanostructured V_2O_5 thin films were spay deposited on the glass substrates. Initial solutions had different concentrations of 0.025 to 0.1 M [57]. It was found that the sensor fabricated from the solution with initial concentration of 0.1 M had the highest sensing performance. In this sensor, a high surface area due to high surface roughness was obtained which significantly increased the response to xylene gas. Initially in air, oxygen molecules were adsorbed on the surface of the gas sensor as follows:

$$O_2(g) \rightarrow O_2(ads) \quad (4)$$

$$O_2(ads) + e^- \rightarrow O_2^- (ads) \quad (5)$$

$$O_2^-(ads) + e^- \rightarrow 2O^-(ads) \quad (6)$$

$$O^-(ads) + e^- \rightarrow O^{2-}(ads) \quad (7)$$

Then, the following reaction occurred between the xylene and adsorbed oxygen species:

$$C_8H_{10} + 21O_2^- \rightarrow 16CO_2 + 10H_2O + 21e^- \quad (8)$$

Accordingly, the conductivity of the sensor significantly increased, and led to the appearance of a sensing signal. To demonstrate the formation of CO_2 as a byproduct of sensing reactions, a lime water test was conducted. Initially, a solution of saturated $Ca(OH)_2$ with a clear color was prepared. Upon introduction of xylene into the gas chamber, due to the conversion of saturated $Ca(OH)_2$ into $CaCO_3$, its color was changed to milky, confirming the release of CO_2 as a byproduct of sensing reaction [53].

Jin et al. [58], prepared random alignment V_2O_5 NW and V_2O_5 NW microyarn gas sensors for ethanol sensing studies. The response of the microyarn gas sensors reached the maximum value of 9.09 for 1000 ppm ethanol at 330 °C, which was ~3.5 times higher than that of the random alignment NWs (Figure 7). For the random oriented NWs, electrons in their pathways encountered a network of NWs. Accordingly, they should overcome two potential barriers namely (i) electrode–V_2O_5 barriers, and (ii) V_2O_5 –V_2O_5 homojunctions barriers. For the microyarn gas sensor, the agglomeration of NWs was prevented effectively, resulting in the exposing of a larger surface area to target gas. In addition, the orderly assembled yarns provided a direct path for flow of electrons, leading to a high response to ethanol gas.

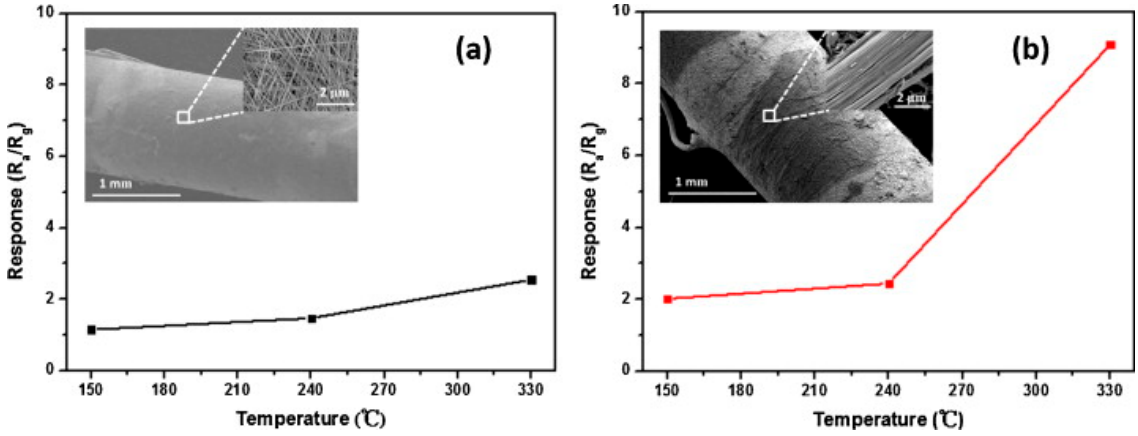

Figure 7. Response curve of sensors to 1000 ppm ethanol at 330 °C: (**a**) randomly oriented V_2O_5 NWs and (**b**) orderly assembled V_2O_5 NW microyarns [58].

Plasma focus (PF) is a pulse plasma device which generates high temperatures and high density of a plasma column very fast. PF has a high deposition rate, energetic deposition process as well as the ability of working in the presence of reactive gases. In an attempt, V_2O_5 thin films were prepared by the PF technique using different shots [59]. It was found that the surface morphology of deposited samples had a key role in the gas response of deposited films. A V_2O_5 thin film prepared with ten shots exhibited the highest H_2 gas response among all the gas sensors at 275 °C. The higher response of the optimized gas sensor can be related to the presence of more oxygen vacancies as well as higher surface area as a result of rougher morphology.

Effect of V_2O_5 film thickness also has been investigated. The nanocrystalline V_2O_5 thin films with NR-like morphology and different thicknesses of 423, 559, 694 and 730 nm were deposited onto the glass substrates using a spray pyrolysis technique. The V_2O_5 film with a thickness 559 nm revealed the highest response (41% to 100 ppm NO_2 at 200 °C) due to the higher surface area [60]. This study shows the need for the optimization of film thickness to achieve the best sensing performance.

Table 1 presents the gas sensing characteristics of pristine V_2O_5 gas sensors, where different morphologies of V_2O_5 prepared using various methods have been successful for sensing of different gases.

Table 1. Gas sensing properties of pristine V_2O_5 gas sensors.

V_2O_5 Morphology	Synthesis Method	Target Gas	Conc. (ppm)	Response (R_a/R_g) or (R_g/R_a)	T (°C)	Response time/Recovery Time(s)	Ref.
Hollow spheres Solid spheres	Solvothermal	C_3H_9N	500 500	9.7 3.08	370	20/83 45/150	[37]
Hollow spheres	Chemical synthesis	H_2	200	2.8	RT	50/10	[38]
Nanoneedles	PVD	C_3H_6O	140	2.35	RT	67/-	[39]
Hierarchical nanostructures	Hydrothermal	C_3H_9N	10–200	1.13-3.57	240	5/28	[42]
Flower-like	Hydrothermal		5	2.25	200	13/13	[43]
Nanorods	CVD	NH_3	100	235 *	400	-/-	[44]
Nanorods	Solvothermal	C_2H_5OH NH_3	500	1.04 1.02	RT	-/-	[45]
Spherical	Precipitation	C_2H_5OH NH_3		1.04 1.06		-/-	[46]

Table 1. *Cont.*

V_2O_5 Morphology	Synthesis Method	Target Gas	Conc. (ppm)	Response (R_a/R_g) or (R_g/R_a)	T (°C)	Response time/Recovery Time(s)	Ref.
Flower-like	Hydrothermal	1-butylamine	100	2.6	140	9/49	[47]
Nanofibers	Electrospinning		9.5	500 *	RT	-/-	[48]
Flower-like Sheet-like	Hydrothermal		100	3.6 2.8	300	25/14 17/14	[49]
Nanofibers	Sol–gel	NH_3	2.1	11 *	200	50/350	[50]
Flower-like	DC sputtering	CH_4	500		100	206/247	[52]
	Hydrothermal	C_8H_{10}		3	300	44/74	[54]
Nano stars	Hydrothermal	He	300	53 *	RT	9/10	[55]
Nanorods	Chemical spray pyrolysis	NO_2	100	24.2 *	200	13/140	[56]
Nanofibers	Chemical spray pyrolysis	C_8H_{10}		27	RT	80/50	[57]
Nanowires	Melt quenching	C_2H_5OH	1000	9.09	330	-/-	[58]
Thin film	Plasma focus method	H_2		50 *	275	-/-	[59]
	Chemical spray pyrolysis	NO_2	100	41 *	200	20/150	[60]

* Response = $\frac{\Delta R}{Ra} \times 100$; RT: Room temperature; PVD: Physical vapor deposition; CVD: Chemical vapor deposition.

3. Decorated/Doped V_2O_5 Gas Sensors

Based on the above section about pristine V_2O_5 gas sensors, pristine V_2O_5 nanostructures suffer from low sensitivity and selectivity, which hinder their applications for sensing applications [61]. Accordingly, different strategies, such as p-n heterojunction formation [62], n-n heterojunction formation [63,64] and noble metal decoration [65] have been proposed to enhance their sensing properties. In the following section, we will discuss different aspects of such gas sensors based on V_2O_5 nanostructures.

V_2O_5 decoration is a good strategy to enhance the sensing properties of gas sensors. V_2O_5-decorated α-Fe_2O_3 composite NRs were prepared by an electrospinning technique and they had a high surface area of 30.5 m^2/g. The composite exhibited a response (R_a/R_g) of 9 to 100 ppm diethylamine along with good selectivity to diethylamine gas and a fast response time of 2 s at 350 °C [66]. Improved sensing performance was related to the formation of V_2O_5-Fe_2O_3 heterojunctions and catalytic effect of V_2O_5 to diethylamine.

In another study, Ko et al. [67], decorated V_2O_5 nanoislands on the surface of SnO_2 NWs using different cycles of atomic layer deposition (ALD) and the effect of ALD cycles was investigated. It was found that the sensor with 50 ALD cycles showed the highest response to NO_2 gas. In particular its response to 200 ppb NO_2 was ~3.7 at 250 °C. Figure 8a,b displays the energy band diagrams of the sensing layer, before and after equilibrium. V_2O_5 nanoislands on the SnO_2 NWs improved the sensing response by generation of depletion layers at the V_2O_5/SnO_2 interface and modulation of the SnO_2 conduction channel. However, the excess amount of V_2O_5 nanoislands deposited by a higher number of ALD cycles, resulted in the decrease in sensor response. The density functional theory (DFT) calculations shown in Figure 8c, regarding NO_2 adsorption energies of both the SnO_2 (1 0 1) and V_2O_5 (0 0 1) planes were −1.5 eV and 1.0 eV, respectively. Thus, it was concluded that the SnO_2 surface was more favorable for adsorption of NO_2 relative to V_2O_5. Therefore, the excess amount of V_2O_5 on the surface of SnO_2 (Figure 8d), resulted in a significant decrease in the gas response due to limited exposure of SnO_2 to NO_2 gas.

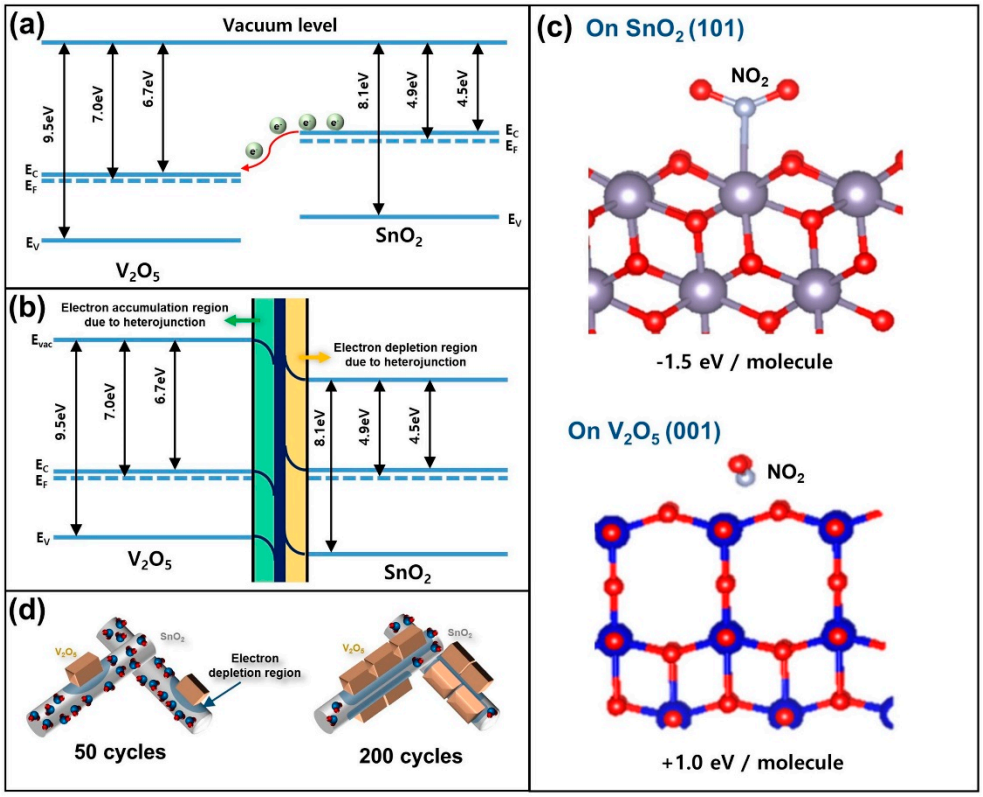

Figure 8. (**a**,**b**) Energy band diagrams of SnO_2-V_2O_5 before and after contact in air. (**c**) NO_2 adsorption on SnO_2 (101) V_2O_5 (001) surfaces. (**d**) Effect of number of ALD cycles and amount of V_2O_5 on the surface of SnO_2 [67].

Porous silicon (PS) is a good candidate for sensing studies due to its offering of a high surface area and a porous structure. In addition it can be simply prepared by a chemical etching process [68]. Therefore, composites between V_2O_5 and PS can be promising for gas sensing studies. In a relevant study, thin V films were decorated on the PS by sputtering at different times of 30 and 60 min and then, the samples were annealed at 600 °C [69]. The PS/V_2O_5 NRs structure provided a better response than pristine PS at 25 °C, and the sensor sputtered for 60 min exhibited the highest response of 7.4 to 2 ppm NO_2 gas. Both the PS and V_2O_5 NRs had plenty of dangling bonds, oxygen vacancies and defects, leading to high adsorption of oxygen molecules even at room temperature. In the interfaces between PS and V_2O_5, p-n heterojunctions formed and, upon exposure to NO_2 gas, the significant modulation of electrical resistance in the heterojunctions led to the appearance of a sensing signal.

Graphene and its derivations such as graphene oxide and reduced graphene oxide have high surface areas and unique electrical properties which can be beneficial for gas sensing studies [70,71]. The initial resistance of the GO is high, limiting its practical applications in pristine form [72,73]. However, after the reduction GO to RGO, there are some defects, vacancies and functional groups which are useful for gas sensing applications [74]. In a relevant study, an RGO surface was decorated with Mn_3O_4 and V_2O_5 NOs via a hydrothermal method for detection of H_2 gas at 30 °C. The sensor showed a high response ($\Delta R/R_a \times 100$) of 174% to 50 ppm H_2 gas at room temperature. The sheet-like structure of RGO provided a large surface area for gas sensing reactions. In addition, because of the formation of p-n (RGO-V_2O_5) and p-p (RGO-Mn_3O_4) heterojunctions, significant modulation of resistance in the presence of H_2 occurred, resulting in the generation of a sensing signal [75]. In another study, a V_2O_5 film was prepared by a reactive sputtering technique and then, RGO was decorated over the V_2O_5 thin film by a drop casting method for NO_2 sensing studies. The sensor showed a response of 50.7% to 100 ppm NO_2 gas at 150 °C. However, its recovery time was long (778 s). Formation and modulation of the p-n heterojunction at the interface of RGO and V_2O_5 was the main reason for the

detection of NO_2 gas. Moreover, the presence of active sites such as oxygen functional groups on the RGO surface improved the sensing response [76].

Not only can V_2O_5-decoration be a useful technique to enhance the gas sensing properties, but decoration of other metal oxides or noble metals on the surface of gas sensor can also be a good technique to improve the gas sensing properties of V_2O_5-based gas sensors. A P-type CuO with excellent catalytic activity is extensively used for sensing studies [77]. The work function of CuO is 5.3 eV, which is different to that of V_2O_5 (4.7 eV). Therefore, when heterojunctions form between the CuO and V_2O_5, enhanced gas response can be expected. In this context, hollow nanostructures using CuO decorated V_2O_5 nano-strings of pearls were fabricated through an electrospinning method. The V_2O_5/CuO sensors demonstrated a response (R_a/R_g) of 8.8 to 500 ppm acetone at 440 °C, which was more than three times higher than that of bare V_2O_5 NFs. The improved performance was related to the generation of CuO/V_2O_5 p-n heterojunctions, which provided plenty of resistance modulation sources and upon exposure to acetone gas higher response was resulted [78].

In another relevant study, CuO NPs-decorated V_2O_5 NWs were fabricated by a two-step process, by combination of hydrothermal and wet-deposition methods [79]. The H_2S response of the sensor was 31.86 to 23 ppm of H_2S gas at 220 °C. The high response was related to the p-n junction formed at the interface between CuO and V_2O_5 along with conversion of CuO to metallic-like CuS. In air, the potential barriers were formed in the interfaces between two materials. Upon injection of H_2S, the CuO was converted to CuS with metallic-like conductivity. Accordingly, the height of the junction was significantly decreased, resulting in great modulation of electrical resistance and a high response to H_2S resulted.

SnO_2 NPs-decorated V_2O_5 NWs were realized by a two-step mild hydrothermal route for sensing applications [80]. The sensor showed a response of ~16 to 1000 ppm ethanol which was three times higher than that of pristine V_2O_5 NWs. The higher response of the gas sensor was explained on the basis of formation of heterojunctions between the SnO_2 and V_2O_5, formation of V_2O_5- V_2O_5 homojunctions due to networked nature of synthesized V_2O_5 NWs, high intrinsic sensing properties of SnO_2 NPs and efficient electron transport along the conduction band of V_2O_5 NWs.

Fe_2O_3-decorated V_2O_5 nanotubes were fabricated using a two-step rheological phase reaction and hydrothermal synthesis for sensing studies. The sensor exhibited a response (R_a/R_g) of 2.2 to 1000 ppm ethanol which was slightly higher than the response to toluene gas od the same concentration with a response of 1.5 at 270 °C [81]. However, the authors did not report selectivity of gas sensors over different gases.

Ozone (O_3) is a strong oxidizing gas that can affect the human body severely. TiO_2 NPs were decorated on V_2O_5 NWs via a hydrothermal method for ozone sensing studies. The pristine TiO_2 sensor was not sensitive to O_3 gas. The sensor showed a response of 2.6 ($\Delta R/R_a$) to 1.25 ppm O_3 gas at 300 °C, while almost no response was recorded for the pristine TiO_2 sensor. When the sensor was exposed to O_3 gas, following reactions took place [82]:

$$O_{3(g)}+e^- \rightarrow O^-_{3(ads)} \quad (9)$$

$$O^-_{3(ads)}+O^-_{(ads)}+2e^- \rightarrow O_{2(g)}+2O^-_2(ads) \quad (10)$$

As a result, electrons were extracted from the surface of the gas sensor and changed the height of potential barriers formed between TiO_2 and V_2O_5. This led to a generation of a sensing signal to O_3 gas.

Noble metal decoration is also a good strategy to enhance sensing properties [83]. V_2O_5 nanoflowers were synthesized via a hydrothermal route and then they were decorated with Au NPs at different loading levels of 0.5, 1.5, 2.5, 3.5, and 5 mol%. The optimal gas sensor with a 3.5 mol% Au NPs showed a response (R_a/R_g) of ~7.3 to 100 ppm 1-buthylamine at 240 °C, while the response of the pristine gas sensor to the same concentration of 1-buthylamine gas was only 3 at 300 °C. Since there

was negligible difference in the surface area among all samples, the enhanced gas sensing response for the sensor with 3.5 mol% Au NPs was related to the chemical and electronic effects of Au [84].

In another study using the decoration of noble metals on the surface of V_2O_5, Sanger et al. [85], deposited a Pd/V_2O_5 thin film by DC magnetron reactive sputtering for H_2 gas sensing studies. The deposition of V and Pd were performed at 300 °C for 60 min and 10 s, respectively. A very fast response within 6 s, recovery time of 21 s and a response of 5 was recorded for 100 ppm of H_2.

A gasochromic mechanism was proposed for H_2 gas sensing, where, based on XPS studies, the formation of vanadium bronze ($H_xV_2O_5$) was confirmed by an increase in the intensity of the V^{4+} peaks. Furthermore, Pd dissociated hydrogen molecules into atomic hydrogen and subsequently, they were spilled over onto the V_2O_5 surface, to react with adsorbed oxygen species. Thus, V_2O_5 was converted to vanadium bronze, with a simultaneous color change from light yellow to light blue.

Generally, only one type of material is used for decoration. However, co-decoration can have more effect on the gas response of gas sensors. For example, it was found that co-decoration of V_2O_5 and Pd on the surface of SnO_2 NPs can significantly enhance both the response of gas sensor to H_2 gas and at the same time, it can decrease the recovery time of the gas sensor [86]. It was reported that during the recovery time, re-oxidization of V_2O_5 led to increase in the recovery time. However, the presence of Pd, significantly decreased the recovery time due to the fact that Pd not only was effective in hydroxyl desorption and oxygen re-adsorption on the SnO_2 surface but also it significantly accelerated the re-oxidization of V_2O_5. Accordingly, co-loading of V_2O_5 and Pd resulted in a complementarity effect, which improves the sensor response and recovery time at the same time.

Benzene (C_6H_6) is extensively used as an organic solvent. However, it is a toxic substance, leading to leukemia and lymphomas diseases [87]. V_2O_5 as dopant has been rarely used for gas sensing studies. A series of pristine and V_2O_5-doped SnO_2 NFs (V_2O_5/SnO_2 = 0.5, 1, 2.5 and 5 mol%) were synthesized via electrospinning for benzene sensing studies [88]. It was reported that the sensor with V_2O_5/SnO_2 = 1 exhibited the highest response to benzene (6.32 at 325 °C to 25 ppm). V_2O_5 catalyzed benzene into maleic anhydride and activated the benzene ring, resulting in better interaction with adsorbed oxygen species. However, a decrease in gas response for higher doping levels was related to the evaluation of a more compact structure, leading to lower adsorption sites and a lower sensing response.

Table 2 shows the gas sensing properties of decorated or doped V_2O_5-based gas sensors, where different synthesis methods along with different morphologies and various materials have been reported to realize gas sensors for the sensing of toxic gases.

Table 2. Gas sensing properties of decorated or doped V_2O_5-based gas sensors.

Sensor	Synthesis Method	Target Gas	Conc. (ppm)	Response (R_a/R_g) or (R_g/R_a)	Working Temp. (°C)	Response Time/Recovery Time(s)	Ref.
Pd decorated porous Si/V_2O_5 nanopillars	DC sputtering	NO_2	2	4.5	RT	-/-	[62]
Ru-decorated layer structure V_2O_5	Hydrothermal	NH_3	130	4 *	RT	~2/~12	[65]
V_2O_5-decorated α-Fe_2O_3 nanorods	Electrospinning	$C_4H_{11}N$	300	9	350	2/40	[66]
V_2O_5 decorated SnO_2 NWs	VLS/ALD	NO_2	200 ppb	3.6	250	-/-	[67]
Porous Si/V_2O_5 NR composite	Galvanostatic electrochemical etching	NO_2	2	7.4	RT	-/-	[69]
rGO/Mn_3O_4/V_2O_5 nanocomposite	Hydrothermal	H_2	50	175	RT	82/92	[75]
Pd-decorated CuO NWs	UV irradiation	H_2S	100	1.962	100	-/-	[76]
V_2O_5/CuO nano-string of pearls	Electrospinning	C_3H_6O	500	9	440	~40/~100	[78]
CuO-decorated V_2O_5 NWs	Hydrothermal and wet-deposition	H_2S	23	31.86	220	130/218	[79]

Table 2. *Cont.*

Sensor	Synthesis Method	Target Gas	Conc. (ppm)	Response (R_a/R_g) or (R_g/R_a)	Working Temp. (°C)	Response Time/Recovery Time(s)	Ref.
SnO_2 NP-decorated V_2O_5 NWs	Hydrothermal	C_2H_5OH	1000	1.3	RT	-/-	[80]
Fe_2O_3 activated V_2O_5 nanotubes	Hydrolysis	C_2H_5OH	1000	2.2	270	-/-	[81]
TiO_2-decorated V_2O_5 NWs	Hydrothermal	O_3	1.25	2.6 *	300	~180/~180	[82]
RGO-decorated V_2O_5 thin film	Reactive sputtering and drop casting	NO_2	100	50.7	150	-/-	[76]
Au NP-decorated V_2O_5	Two-step in-situ reduction of Au and thermal oxidization as V_2O_5	Amines	100	7.5	240	90/35	[84]
Pd-decorated V_2O_5 thin film	DC magnetron reactive sputtering	H_2	100	5.7	100	~6/14.8	[85]
V_2O_5-doped SnO_2 NFs	Electrospinning	C_6H_6	25	6.32	325	3/47	[88]

* Response = $\frac{\Delta R}{Ra} \times 100$; RT: Room temperature; VLS: Vapor-liquid-solid; NR; Nanorod; NP; Nanoparticle; NF; Nanofiber.

4. Nanocomposites/Nanohybrids of V_2O_5 Gas Sensors

Core-shell (C-S) nanocomposites are among the most promising structures for gas sensing studies, as in these structures the interfaces between two different materials are maximized, resulting in significant modulation of electrical resistance upon exposure to target gases [89–91]. Fu et al. [40], synthesized V_2O_5-TiO_2 core-shell (C-S) NPs for NH_3 studies. For pristine V_2O_5 NPs, the surface area was only ~16 m^2/g with a pore size of 12.9 nm, while the BET surface area of V_2O_5@TiO_2 C-S NPs was greatly increased to ~151 m^2/g, and the average pore size was ~6.4 nm. Thus, the significant increase in surface area was an advantage for C-S NPs, which directly affected the gas sensing studies. The C-S sensor showed a response (R_a/R_g) of 8.6 to 100 ppm ammonia at 365 °C. Upon intimate contact between the V_2O_5 and TiO_2, electrons moved from TiO_2 to V_2O_5, resulting in the creation of an electron depletion layer on both sides of the TiO_2 shell layer. Upon injection of NH_3 gas into the gas chamber, the electrons released back caused the narrowing of the electron depletion layers which finally modulated the electrical resistances of the gas sensor. Moreover, based on DFT calculations, the NH_3 molecule showed the lowest adsorption energy (−1.04 eV) on the anatase TiO_2 (101) surface, which explained the higher selectivity of the gas sensor to NH_3 among other tested gases. The optimal sensing temperature of the gas sensor was registered at 365 °C. The reactions on the surface of TiO_2 can be shown as follows:

$$O_2 + 4e^- \rightarrow 2O^{2-} \quad (11)$$

$$2NH_3 + 3O^{2-} \rightarrow N_2 + 3H_2O + 6e^- \quad (12)$$

$$2NH_3 + 4O^{2-} \rightarrow N_2O + 3H_2O + 8e^- \quad (13)$$

$$2NH_3 + 5O^{2-} \rightarrow 2NO + 3H_2O + 10e^- \quad (14)$$

Thus, more electrons can be released when N_xO (x = 1, 2), demonstrating the high response toward NH_3 at elevated temperatures (>300 °C).

In another study related to C-S nanocomposites, V_2O_5/In_2O_3 C-S NRs were prepared using a solid solution synthesis method, followed by a hydrothermal method. In_2O_3 as shell, led to the increase in surface active sites for gas adsorption. The sensor showed a response (R_a/R_g) of 14 to 200 ppm n-propylamine at 190 °C. Higher selectivity of the sensor to n-propylamine was explained on the basis of selective oxidation of n-propylamine.

Additionally, presence of the two types of materials with different reduction-oxidation and acid-base properties affected the selectivity of the gas sensor to n-propylamine [92].

Combination of MoO_3, which has layered structure with V_2O_5 with high catalytic activity can be a good strategy for enhanced gas sensing performance of the MoO_3-V_2O_5 composite.

The $(MoO_3)_{1-x}(V_2O_5)_x$ thin films with x = 0.2, 0.4, 0.6 and 0.8 were prepared using a chemical spray pyrolysis method. For $(MoO_3)_{0.4}(V_2O_5)_{0.6}$ thin film, a gas response of 80% at 200 °C to 100 ppm NO_2 gas was recorded [93]. The sensing layer with a sheet-like morphology and the presence of voids in its layered structure, provides a lot of adsorption sites for NO_2 gas molecules. In addition, NO_2 gas was able to diffuse into the depth parts of gas sensor, resulting in more interaction between the gas molecules and already adsorbed oxygen molecules. In another study which was conducted by the same group, Pd was decorated on the optimal gas sensor, $(MoO_3)_{0.4}(V_2O_5)_{0.6}$ and a higher gas response resulted due to the catalytic effect of Pd and formation of different heterojunctions [94].

Use of conducting polymers (CPs) can greatly decrease the sensing temperature of the resultant composite material. In this regard, Diniz et al. [95] used a poly(*o*-methoxyaniline) (POMA)–V_2O_5 hybrid composite film for NH_3 detection. POMA has an OCH_3 group which can improve the processability of POMA [96]. The function of V_2O_5 was to enhance the structural stability during the doping and dedoping of POMA when exposing it to NH_3 gas. The sensing mechanism is explained as follows. A p-n heterojunction was formed between the POMA–V_2O_5 hybrid and, by interaction with NH_3 gas, the wide of depletion layers and height of potential barriers decreased, resulting in resistance change of the hybrid composite film [95].

Even low concentrations of NH_3 can negatively affect skin and human respiratory organs. This led to the setting of the indoor exposure limit of NH_3 to 25 ppm [97]. Au-loaded flower-like $V_2O_5/CuWO_4$ nanocomposites were synthesized for NH_3 studies. The sensor showed a response (R_a/R_g) of 2.7 to 5 ppm NH_3 at 150 °C, which was higher than the response to other gases. In addition to promising effects of heterojunctions formed between different sensing materials, the Au NPs facilitated the electron flow among the sensing materials and the NH_3 and thus a short response time of 35 s was recorded. In addition, Au NPs catalytically increase the dissociative adsorption of O_2 molecules as O^- species and, in a so-called spillover process, atomic oxygen species moved to the surface of $V_2O_5/CuWO_4$, leading to wider depletion layer and acceleration of the gas reactions on the surface of the sensing layer [98].

Zhang et al. [99] developed a series of SnO_2/V_2O_5 composites for sensing of benzene, toluene, ethyl benzene, and xylene (BTEX) gases. At 270 °C, the sensor with 10 wt% V_2O_5 showed the highest response to BTEX gases. It was reported that V_2O_5 catalyzed oxidation of benzene into a maleic anhydride, implying that V_2O_5 was able to activate the benzene ring, then benzene reacted with the absorbed oxygen species easily on the surface of SnO_2. The sensor response was decreased for the sensor with 20 wt% V_2O_5, which could be due to the fact that the intrinsic response of SnO_2 is higher than that of V_2O_5. In fact, when there is too much V_2O_5, the adsorption sites on the surfaces of SnO_2 decrease, leading to a decrease in sensor response [99].

The effect of the nature of polymer (PVP and PVAc) used for the electrospinning process on the sensing response of of V_2O_5-based gas sensors was investigated. At 260 °C, the V_2O_5/PVP sensor, showed a response ($\Delta R/R_a \times 100$) of ~7 to 0.8 ppm NH_3 gas which was slightly higher than that of the V_2O_5/PVAc sensor. It was reported that the V_2O_5/PVP network was constituted of fibers with a smaller diameter which resulted in larger resistance modulation of the gas sensor. In fact, a larger part of the diameter of fibers with smaller diameters was depleted from electrons and this resulted in more intense resistance modulation upon exposure to target gas [100].

Layered V_2O_5/ZnV_2O_6 nanocomposites were synthesized via a chemical route for ethanol sensing applications [101]. The sensor revealed a response of 4.3 to 100 ppm ethanol at 240 °C. The enhanced sensing properties were related to high mobility of electrons in the layered structure of the gas sensor along with the formation and subsequent modulation of potential barriers between V_2O_5 and ZnV_2O_6 in the presence of ethanol gas. Furthermore, TiO_2/V_2O_5 branched NFs were fabricated by an electrospinning process. The sensor showed a high response (R_a/R_g) of 24.6 to 100 ppm ethanol at 350 °C which was attributed to the high surface area of the branched sensor (33.6 m^2/g) and the synergistic effects between TiO_2 and V_2O_5 upon intimate contact [102].

In another study, the effect of ZnO addition on the room temperature toluene sensing properties of ZnO/V_2O_5 nanocomposite thin films was systematically studied. ZnO/V_2O_5 nanocomposites were deposited using spray pyrolysis for the detection of toluene at 27 °C [103]. The response to toluene was improved by the addition of V_2O_5 to the ZnO thin film and the sensor with a composition of 70 wt% ZnO showed a response of 2.3 to 400 ppm toluene which was the highest response among the gas sensors. In fact, in a part form formation of heterojunctions, the presence of V_2O_5 led to further adsorption of oxygen, and ZnO with intrinsic high sensing properties and high electron mobility also contributed to the sensing signal. Table 3 exhibits the sensing properties of various V_2O_5-based composite gas sensors, where different materials along with various morphologies have been used for sensing of different gases.

Table 3. Gas sensing properties of V_2O_5-based composite gas sensors.

Sensing Material	Synthesis Method	Target Gas	Conc. (Ppm)	Response (R_a/R_g) Or (R_g/R_a)	T (°C)	Response Time/Recovery Time(S)	Ref.
V_2O_5/In_2O_3 core–shells	Hydrothermal	n-propylamine	200	4	190	48/121	[92]
MoO_3-V_2O_5 thin films	Chemical spray pyrolysis	NO_2	120	80 *	200	118/1182	[93]
$(MoO_3)_{0.4}(V_2O_5)_{0.6}$ sheet composite	Chemical spray pyrolysis		100	115		39/453	[94]
Au/V_2O_5/$CuWO_4$ composite	Hydrothermal	NH_3	5	2.7	150	35/33	[98]
SnO_2/V_2O_5 composite	Sol-gel	C_6H_6	200	10.5	275	-/-	[99]
V_2O_5/polyvinyl acetate NF composite	Electrospinning	NH_3	0.8	6 *	260	-/-	[100]
V_2O_5/ZnV_2O_6 nanobelt composite	Chemical route	C_2H_5OH	2000	16.5	240	-/-	[101]
TiO_2/V_2O_5 NF composite	Electrospinning		100	24.6	350	6/7	[102]
ZnO/V_2O_5 thin films	Spray pyrolysis	C_7H_8	400	2.3	27	23/28	[103]

* Response = $\frac{\Delta R}{Ra} \times 100$.

5. Conclusions and Outlook

In this review paper, we discuss different aspects of V_2O_5-based gas sensors. In general, pristine V_2O_5 gas sensors can show response to a variety of gases. In pristine form, V_2O_5 gas sensors with different morphologies can be synthesized by using physical methods such as reactive sputtering or by using chemical methods such as hydrothermal and sol–gel methods. Depending on the surface chemistry, morphology and sensing temperatures, the pristine V_2O_5 gas sensors show different response values to a specific gas. However, in general, the response and selectivity of pristine V_2O_5 gas sensors is poor. To enhance sensing performance of pristine gas sensors, noble metal decoration can be a good strategy. Noble metals such as Au, Pd and Pt can significantly enhance not only the response of gas sensors, but also the selectivity to a specific gas. However, less attention has been paid to systematically optimize the amount of noble metals on the surface of V_2O_5 and most of researchers only investigated the effect of a specific amount of noble metals on the sensing performance. In addition, co-decoration can be also a good strategy to further enhance the sensing properties such as response, selectivity and response and recovery times.

Formation of heterojunctions with n- or p-type materials is another strategy to increase the overall sensing performance. This strategy may be more cost-effective than noble metal decoration. Furthermore, composite making can be performed in one-step avoiding complex procedures associated with noble metal decoration. The height of heterojunction barriers changes upon exposure of gas sensors to target gases, leading to enhanced gas response.

Unfortunately, some aspects of V_2O_5-based gas sensors have not investigated yet. For example, the effects of ion-implantation and UV illumination have not reported yet. Furthermore, there is no report about operation of V_2O_5-based gas sensors in self-heating mode. Moreover, less attention has been paid to nanohybrids between V_2O_5 and CPs, which can significantly decrease the sensing temperature. In spite of great efforts and advances related to the V_2O_5-based gas sensors, the selectivity issue is still a serious problem and more works are necessary to solve it. Therefore, it is expected that

future studies related to V_2O_5-based gas sensors will be directed to explore these expected V_2O_5-based gas sensors.

Author Contributions: Investigation, V.A.; conceptualization and writing—original draft preparation, A.M., H.R.; M.H.S. All authors have read and agreed to the published version of the manuscript.

Funding: This research received no external funding.

Acknowledgments: Thanks to the support of Shiraz University of Technology.

Conflicts of Interest: The authors declare no conflict of interest.

References

1. Le, T.K.; Kang, M.; Kim, S.W. A review on the optical characterization of v_2o_5 micro-nanostructures. *Ceram. Int.* **2019**, *45*, 15781–15798. [CrossRef]
2. Mane, A.A.; Maldar, P.S.; Dabhole, S.H.; Nikam, S.A.; Moholkar, A.V. Effect of substrate temperature on physicochemical and gas sensing properties of sprayed orthorhombic v_2o_5 thin films. *Measurement* **2019**, *131*, 223–234. [CrossRef]
3. Bouzidi, A.; Benramdane, N.; Bresson, S.; Mathieu, C.; Desfeux, R.; Marssi, M.E. X-ray and raman study of spray pyrolysed vanadium oxide thin films. *Vib. Spectrosc.* **2011**, *57*, 182–186. [CrossRef]
4. Su, Q.; Lan, W.; Wang, Y.Y.; Liu, X.Q. Structural characterization of β-v_2o_5 films prepared by dc reactive magnetron sputtering. *Appl. Surf. Sci.* **2009**, *255*, 4177–4179. [CrossRef]
5. Ramana, C.; Hussain, O.; Naidu, B.S.; Reddy, P. Spectroscopic characterization of electron-beam evaporated v2o5 thin films. *Thin Solid Film* **1997**, *305*, 219–226. [CrossRef]
6. Laubach, S.; Schmidt, P.C.; Thißen, A.; Fernandez-Madrigal, F.J.; Wu, Q.-H.; Jaegermann, W.; Klemm, M.; Horn, S. Theoretical and experimental determination of the electronic structure of v_2o_5, reduced v_2o_{5-x} and sodium intercalated nav_2o_5. *Phys. Chem. Chem. Phys.* **2007**, *9*, 2564–2576. [CrossRef]
7. Aawani, E.; Memarian, N.; Dizaji, H.R. Synthesis and characterization of reduced graphene oxide–v_2o_5 nanocomposite for enhanced photocatalytic activity under different types of irradiation. *J. Phys. Chem. Solids* **2019**, *125*, 8–15. [CrossRef]
8. Rathika, R.; Kovendhan, M.; Joseph, D.P.; Pachaiappan, R.; Kumar, A.S.; Vijayarangamuthu, K.; Venkateswaran, C.; Asokan, K.; Jeyakumar, S.J. Tailoring the properties of spray deposited v_2o_5 thin films using swift heavy ion beam irradiation. *Nucl. Eng. Technol.* **2020**. [CrossRef]
9. Hou, T.-F.; Johar, M.A.; Boppella, R.; Hassan, M.A.; Patil, S.J.; Ryu, S.-W.; Lee, D.-W. Vertically aligned one-dimensional zno/v_2o_5 core–shell hetero-nanostructure for photoelectrochemical water splitting. *J. Energy Chem.* **2020**, *49*, 262–274. [CrossRef]
10. Slewa, L.H.; Abbas, T.A.; Ahmed, N.M. Effect of sn doping and annealing on the morphology, structural, optical, and electrical properties of 3d (micro/nano) v_2o_5 sphere for high sensitivity ph-egfet sensor. *Sens. Actuators B Chem.* **2020**, *305*, 127515. [CrossRef]
11. Abd-Alghafour, N.M.; Ahmed, N.M.; Hassan, Z.; Almessiere, M.A.; Bououdina, M.; Al-Hardan, N.H. High sensitivity extended gate effect transistor based on v_2o_5 nanorods. *J. Mater. Sci. Mater. Electron.* **2017**, *28*, 1364–1369. [CrossRef]
12. Yin, Z.; Xu, J.; Ge, Y.; Jiang, Q.; Zhang, Y.; Yang, Y.; Sun, Y.; Hou, S.; Shang, Y.; Zhang, Y. Synthesis of v_2o_5 microspheres by spray pyrolysis as cathode material for supercapacitors. *Mater. Res. Express* **2018**, *5*, 036306. [CrossRef]
13. Deepak Raj, P.; Gupta, S.; Sridharan, M. Studies on nanostructured v_2o_5/v/v_2o_5 films for un-cooled ir detector application. *J. Mater. Sci. Mater. Electron.* **2016**, *27*, 7494–7500. [CrossRef]
14. Abd-Alghafour, N.M.; Ahmed, N.M.; Hassan, Z. Fabrication and characterization of v_2o_5 nanorods based metal–semiconductor–metal photodetector. *Sens. Actuators A Phys.* **2016**, *250*, 250–257. [CrossRef]
15. Kim, D.; Yun, J.; Lee, G.; Ha, J.S. Fabrication of high performance flexible micro-supercapacitor arrays with hybrid electrodes of mwnt/v_2o_5 nanowires integrated with a sno_2 nanowire uv sensor. *Nanoscale* **2014**, *6*, 12034–12041. [CrossRef]
16. Singh, N.; Umar, A.; Singh, N.; Fouad, H.; Alothman, O.Y.; Haque, F.Z. Highly sensitive optical ammonia gas sensor based on sn doped v_2o_5 nanoparticles. *Mater. Res. Bull.* **2018**, *108*, 266–274. [CrossRef]

17. Santos, M.C.; Hamdan, O.H.C.; Valverde, S.A.; Guerra, E.M.; Bianchi, R.F. Synthesis and characterization of v_2o_5/pani thin films for application in amperometric ammonia gas sensors. *Org. Electron.* **2019**, *65*, 116–120. [CrossRef]
18. Wang, C.; Li, X.; Yuan, Y.; Wang, B.; Huang, J.; Xia, F.; Zhang, H.; Xiao, J. Effects of sintering temperature on sensing properties of v_2o_5-wo_3-tio_2 electrode for potentiometric ammonia sensor. *Sens. Actuators B Chem.* **2017**, *241*, 268–275. [CrossRef]
19. Alam, M.M.; Uddin, M.T.; Asiri, A.M.; Rahman, M.M.; Islam, M.A. Development of reproducible thiourea sensor with binary sno_2/v_2o_5 nanomaterials by electrochemical method. *Arab. J. Chem.* **2020**, *13*, 5406–5416. [CrossRef]
20. Rajesh, K.; Santhanalakshmi, J. Design and development of graphene intercalated v_2o_5 nanosheets based electrochemical sensors for effective determination of potentially hazardous 3,5–dichlorophenol. *Mater. Chem. Phys.* **2017**, *199*, 497–507. [CrossRef]
21. Zhang, H.; Zhang, L.; Hu, J.; Cai, P.; Lv, Y. A cataluminescence gas sensor based on nanosized v_2o_5 for tert-butyl mercaptan. *Talanta* **2010**, *82*, 733–738. [CrossRef] [PubMed]
22. Karthikeyan, P.S.; Dhivya, P.; Deepak Raj, P.; Sridharan, M. V_2o_5 thin film for 2-propanol vapor sensing. *Mater. Today Proc.* **2016**, *3*, 1510–1516. [CrossRef]
23. Imawan, C.; Steffes, H.; Solzbacher, F.; Obermeier, E. Structural and gas-sensing properties of v_2o_5–moo_3 thin films for h_2 detection. *Sens. Actuators B Chem.* **2001**, *77*, 346–351. [CrossRef]
24. Chen, C.L.; Dong, C.L.; Ho, Y.K.; Chang, C.C.; Wei, D.H.; Chan, T.C.; Chen, J.L.; Jang, W.L.; Hsu, C.C.; Kumar, K.; et al. Electronic and atomic structures of gasochromic v_2o_5 films. *EPL (Europhys. Lett.)* **2013**, *101*, 17006. [CrossRef]
25. Tadeo, I.J.; Parasuraman, R.; Krupanidhi, S.B.; Umarji, A.M. Enhanced humidity responsive ultrasonically nebulised v_2o_5 thin films. *Nano Express* **2020**, *1*, 010005. [CrossRef]
26. Schneider, K.; Lubecka, M.; Czapla, A. V_2o_5 thin films for gas sensor applications. *Sens. Actuators B Chem.* **2016**, *236*, 970–977. [CrossRef]
27. Vasanth Raj, D.; Ponpandian, N.; Mangalaraj, D.; Viswanathan, C. Effect of annealing and electrochemical properties of sol–gel dip coated nanocrystalline v_2o_5 thin films. *Mater. Sci. Semicond. Process.* **2013**, *16*, 256–262. [CrossRef]
28. Gandasiri, R.; Sreelatha, C.J.; Nagaraju, P.; Vijayakumar, Y. Effect of annealing temperature on micro-structural, optical and electrical characterization of nanostructured v_2o_5 thin films prepared by spray pyrolysis technique. *Phys. B Condens. Matter* **2019**, *572*, 220–224. [CrossRef]
29. Thangarasu, R.; Thangavel, E.; Chandrasekaran, J.; Balasundaram, O.N. Synthesis, characterization and gas sensing performance of v_2o_5 nano-structure on pet substrate. *J. Mater. Sci. Mater. Electron.* **2019**, *30*, 4238–4249. [CrossRef]
30. Yıldırım, M.A.; Tuna Yıldırım, S.; Çağirtekin, A.O.; Karademir, M.; Karaduman Er, I.; Coşkun, A.; Ateş, A.; Acar, S. The effect of deposition time on the structural, morphological and h2s gas sensing properties of the v_2o_5 nanostructures deposited by hydrothermal method. *J. Mater. Sci. Mater. Electron.* **2019**, *30*, 12215–12223. [CrossRef]
31. Mirzaei, A.; Leonardi, S.G.; Neri, G. Detection of hazardous volatile organic compounds (vocs) by metal oxide nanostructures-based gas sensors: A review. *Ceram. Int.* **2016**, *42*, 15119–15141. [CrossRef]
32. Mirzaei, A.; Neri, G. Microwave-assisted synthesis of metal oxide nanostructures for gas sensing application: A review. *Sens. Actuators B Chem.* **2016**, *237*, 749–775. [CrossRef]
33. Amiri, V.; Roshan, H.; Mirzaei, A.; Neri, G.; Ayesh, A.I. Nanostructured metal oxide-based acetone gas sensors: A review. *Sensors* **2020**, *20*, 3096. [CrossRef] [PubMed]
34. Mirzaei, A.; Lee, J.-H.; Majhi, S.M.; Weber, M.; Bechelany, M.; Kim, H.W.; Kim, S.S. Resistive gas sensors based on metal-oxide nanowires. *J. Appl. Phys.* **2019**, *126*, 241102. [CrossRef]
35. Mirzaei, A.; Janghorban, K.; Hashemi, B.; Bonyani, M.; Leonardi, S.G.; Neri, G. A novel gas sensor based on ag/fe2o3 core-shell nanocomposites. *Ceram. Int.* **2016**, *42*, 18974–18982. [CrossRef]
36. Mounasamy, V.; Mani, G.K.; Madanagurusamy, S. Vanadium oxide nanostructures for chemiresistive gas and vapour sensing: A review on state of the art. *Microchim. Acta* **2020**, *187*, 1–29. [CrossRef] [PubMed]

37. Wu, M.; Zhang, X.; Gao, S.; Cheng, X.; Rong, Z.; Xu, Y.; Zhao, H.; Huo, L. Construction of monodisperse vanadium pentoxide hollow spheres via a facile route and triethylamine sensing property. *CrystEngComm* **2013**, *15*, 10123–10131. [CrossRef]
38. Wang, Y.-T.; Whang, W.-T.; Chen, C.-H. Hollow v_2o_5 nanoassemblies for high-performance room-temperature hydrogen sensors. *ACS Appl. Mater. Interfaces* **2015**, *7*, 8480–8487. [CrossRef]
39. Hakim, S.A.; Liu, Y.; Zakharova, G.S.; Chen, W. Synthesis of vanadium pentoxide nanoneedles by physical vapour deposition and their highly sensitive behavior towards acetone at room temperature. *RSC Adv.* **2015**, *5*, 23489–23497. [CrossRef]
40. Li, Y.; Liu, J.; Zhang, J.; Liang, X.; Zhang, X.; Qi, Q. Deposition of in_2o_3 nanofibers on polyimide substrates to construct high-performance and flexible trimethylamine sensor. *Chin. Chem. Lett.* **2019**. [CrossRef]
41. Zhang, J.; Song, P.; Li, Z.; Zhang, S.; Yang, Z.; Wang, Q. Enhanced trimethylamine sensing performance of single-crystal moo_3 nanobelts decorated with au nanoparticles. *J. Alloys Compd.* **2016**, *685*, 1024–1033. [CrossRef]
42. Wang, D.; Gu, K.; Zhao, Q.; Zhai, C.; Yang, T.; Lu, Q.; Zhang, J.; Zhang, M. Synthesis and trimethylamine sensing properties of spherical v_2o_5 hierarchical structures. *New J. Chem.* **2018**, *42*, 14188–14193. [CrossRef]
43. Meng, D.; Si, J.; Wang, M.; Wang, G.; Shen, Y.; San, X.; Meng, F. In-situ growth of v_2o_5 flower-like structures on ceramic tubes and their trimethylamine sensing properties. *Chin. Chem. Lett.* **2019**. [CrossRef]
44. Akande, A.A.; Mosuang, T.; Ouma, C.N.M.; Benecha, E.M.; Tesfamichael, T.; Roro, K.; Machatine, A.G.J.; Mwakikunga, B.W. Ammonia gas sensing characteristics of v_2o_5 nanostructures: A combined experimental and ab initio density functional theory approach. *J. Alloys Compd.* **2020**, *821*, 153565. [CrossRef]
45. Dhayal Raj, A.; Pazhanivel, T.; Suresh Kumar, P.; Mangalaraj, D.; Nataraj, D.; Ponpandian, N. Self assembled v_2o_5 nanorods for gas sensors. *Curr. Appl. Phys.* **2010**, *10*, 531–537. [CrossRef]
46. Dhayal Raj, A.; Suresh Kumar, P.; Yang, Q.; Mangalaraj, D. Synthesis and gas sensors behavior of surfactants free v_2o_5 nanostructure by using a simple precipitation method. *Phys. E Low-Dimens. Syst. Nanostructures* **2012**, *44*, 1490–1494. [CrossRef]
47. Yang, T.; Yu, H.; Xiao, B.; Li, Z.; Zhang, M. Enhanced 1-butylamine gas sensing characteristics of flower-like v_2o_5 hierarchical architectures. *J. Alloys Compd.* **2017**, *699*, 921–927. [CrossRef]
48. Raible, I.; Burghard, M.; Schlecht, U.; Yasuda, A.; Vossmeyer, T. V_2o_5 nanofibres: Novel gas sensors with extremely high sensitivity and selectivity to amines. *Sens. Actuators B Chem.* **2005**, *106*, 730–735.
49. Yang, X.H.; Xie, H.; Fu, H.T.; An, X.Z.; Jiang, X.C.; Yu, A.B. Synthesis of hierarchical nanosheet-assembled v_2o_5 microflowers with high sensing properties towards amines. *RSC Adv.* **2016**, *6*, 87649–87655. [CrossRef]
50. Modafferi, V.; Panzera, G.; Donato, A.; Antonucci, P.L.; Cannilla, C.; Donato, N.; Spadaro, D.; Neri, G. Highly sensitive ammonia resistive sensor based on electrospun v_2o_5 fibers. *Sens. Actuators B Chem.* **2012**, *163*, 61–68. [CrossRef]
51. Gross, P.-A.; Jaramillo, T.; Pruitt, B. Cyclic-voltammetry-based solid-state gas sensor for methane and other voc detection. *Anal. Chem.* **2018**, *90*, 6102–6108. [CrossRef] [PubMed]
52. Mounasamy, V.; Mani, G.K.; Ponnusamy, D.; Tsuchiya, K.; Reshma, P.R.; Prasad, A.K.; Madanagurusamy, S. Investigation on ch_4 sensing characteristics of hierarchical v_2o_5 nanoflowers operated at relatively low temperature using chemiresistive approach. *Anal. Chim. Acta* **2020**, *1106*, 148–160. [CrossRef]
53. Kim, B.-Y.; Ahn, J.H.; Yoon, J.-W.; Lee, C.-S.; Kang, Y.C.; Abdel-Hady, F.; Wazzan, A.A.; Lee, J.-H. Highly selective xylene sensor based on nio/$nimoo_4$ nanocomposite hierarchical spheres for indoor air monitoring. *ACS Appl. Mater. Interfaces* **2016**, *8*, 34603–34611. [CrossRef] [PubMed]
54. Cao, P.; Gui, X.; Navale, S.T.; Han, S.; Xu, W.; Fang, M.; Liu, X.; Zeng, Y.; Liu, W.; Zhu, D.; et al. Design of flower-like v_2o_5 hierarchical nanostructures by hydrothermal strategy for the selective and sensitive detection of xylene. *J. Alloys Compd.* **2020**, *815*, 152378. [CrossRef]
55. Chauhan, P.S.; Bhattacharya, S. Highly sensitive $v_2o_5{\cdot}1.6h_2o$ nanostructures for sensing of helium gas at room temperature. *Mater. Lett.* **2018**, *217*, 83–87. [CrossRef]
56. Mane, A.A.; Suryawanshi, M.P.; Kim, J.H.; Moholkar, A.V. Fast response of sprayed vanadium pentoxide (v_2o_5) nanorods towards nitrogen dioxide (no_2) gas detection. *Appl. Surf. Sci.* **2017**, *403*, 540–550. [CrossRef]

57. Vijayakumar, Y.; Mani, G.K.; Ponnusamy, D.; Shankar, P.; Kulandaisamy, A.J.; Tsuchiya, K.; Rayappan, J.B.B.; Ramana Reddy, M.V. V_2O_5 nanofibers: Potential contestant for high performance xylene sensor. *J. Alloys Compd.* **2018**, *731*, 805–812. [CrossRef]
58. Jin, W.; Yan, S.; An, L.; Chen, W.; Yang, S.; Zhao, C.; Dai, Y. Enhancement of ethanol gas sensing response based on ordered v_2o_5 nanowire microyarns. *Sens. Actuators B Chem.* **2015**, *206*, 284–290. [CrossRef]
59. Panahi, N.; Shirazi, M.; Hosseinnejad, M.T. Fabrication, characterization and hydrogen gas sensing performance of nanostructured v_2o_5 thin films prepared by plasma focus method. *J. Mater. Sci. Mater. Electron.* **2018**, *29*, 13345–13353. [CrossRef]
60. Mane, A.A.; Moholkar, A.V. Effect of film thickness on no_2 gas sensing properties of sprayed orthorhombic nanocrystalline v_2o_5 thin films. *Appl. Surf. Sci.* **2017**, *416*, 511–520. [CrossRef]
61. Fu, H.; Jiang, X.; Yang, X.; Yu, A.; Su, D.; Wang, G. Glycothermal synthesis of assembled vanadium oxide nanostructures for gas sensing. *J. Nanopart. Res.* **2012**, *14*, 871. [CrossRef]
62. Qiang, X.; Hu, M.; Zhou, L.; Liang, J. Pd nanoparticles incorporated porous silicon/v_2o_5 nanopillars and their enhanced p-type no_2-sensing properties at room temperature. *Mater. Lett.* **2018**, *231*, 194–197. [CrossRef]
63. Bolokang, A.S.; Motaung, D.E. Reduction-oxidation of v_2o_5-wo_3 nanostructured by ball milling and annealing: Their improved h_2s gas sensing performance. *Appl. Surf. Sci.* **2019**, *473*, 164–173. [CrossRef]
64. Liang, Y.-C.; Cheng, Y.-R. Combinational physical synthesis methodology and crystal features correlated with oxidizing gas detection ability of one-dimensional zno–vox crystalline hybrids. *CrystEngComm* **2015**, *17*, 5801–5807. [CrossRef]
65. Birajdar, S.N.; Hebalkar, N.Y.; Pardeshi, S.K.; Kulkarni, S.K.; Adhyapak, P.V. Ruthenium-decorated vanadium pentoxide for room temperature ammonia sensing. *RSC Adv.* **2019**, *9*, 28735–28745. [CrossRef]
66. Zhang, H.; Luo, Y.; Zhuo, M.; Yang, T.; Liang, J.; Zhang, M.; Ma, J.; Duan, H.; Li, Q. Diethylamine gas sensor using v_2o_5-decorated α-fe_2o_3 nanorods as a sensing material. *RSC Adv.* **2016**, *6*, 6511–6515. [CrossRef]
67. Ko, W.C.; Kim, K.M.; Kwon, Y.J.; Choi, H.; Park, J.K.; Jeong, Y.K. Ald-assisted synthesis of v_2o_5 nanoislands on sno_2 nanowires for improving no_2 sensing performance. *Appl. Surf. Sci.* **2020**, *509*, 144821. [CrossRef]
68. Ozdemir, S.; Gole, J.L. The potential of porous silicon gas sensors. *Curr. Opin. Solid State Mater. Sci. Semicond. Process.* **2007**, *11*, 92–100. [CrossRef]
69. Yan, W.; Hu, M.; Wang, D.; Li, C. Room temperature gas sensing properties of porous silicon/v_2o_5 nanorods composite. *Appl. Surf. Sci.* **2015**, *346*, 216–222. [CrossRef]
70. Chatterjee, S.G.; Chatterjee, S.; Ray, A.K.; Chakraborty, A.K. Graphene–metal oxide nanohybrids for toxic gas sensor: A review. *Sens. Actuators B Chem.* **2015**, *221*, 1170–1181. [CrossRef]
71. Meng, F.-L.; Guo, Z.; Huang, X.-J. Graphene-based hybrids for chemiresistive gas sensors. *TrAC Trends Anal. Chem.* **2015**, *68*, 37–47. [CrossRef]
72. Toda, K.; Furue, R.; Hayami, S. Recent progress in applications of graphene oxide for gas sensing: A review. *Anal. Chim. Acta* **2015**, *878*, 43–53. [CrossRef]
73. Wang, T.; Huang, D.; Yang, Z.; Xu, S.; He, G.; Li, X.; Hu, N.; Yin, G.; He, D.; Zhang, L. A review on graphene-based gas/vapor sensors with unique properties and potential applications. *Nano-Micro Lett.* **2016**, *8*, 95–119. [CrossRef] [PubMed]
74. Lu, G.; Ocola, L.E.; Chen, J. Reduced graphene oxide for room-temperature gas sensors. *Nanotechnology* **2009**, *20*, 445502. [CrossRef]
75. Amarnath, M.; Heiner, A.; Gurunathan, K. Surface bound nanostructures of ternary r-go/ mn_3o_4/v_2o_5 system for room temperature selectivity of hydrogen gas. *Ceram. Int.* **2020**, *46*, 7336–7345. [CrossRef]
76. Bhati, V.S.; Sheela, D.; Roul, B.; Raliya, R.; Biswas, P.; Kumar, M.; Roy, M.S.; Nanda, K.K.; Krupanidhi, S.B.; Kumar, M. No_2 gas sensing performance enhancement based on reduced graphene oxide decorated v_2o_5 thin films. *Nanotechnology* **2019**, *30*, 224001. [CrossRef] [PubMed]
77. Kim, J.-Y.; Lee, J.-H.; Kim, J.-H.; Mirzaei, A.; Woo Kim, H.; Kim, S.S. Realization of h_2s sensing by pd-functionalized networked cuo nanowires in self-heating mode. *Sens. Actuators B Chem.* **2019**, *299*, 126965. [CrossRef]
78. Wu, J.; Xing, X.; Zhu, Z.; Zheng, L.; Chen, J.; Wang, C.; Yang, D. Electrospun hollow cuo modified v_2o_5 nano-string of pearls with improved acetone sensitivity. *Chem. Phys. Lett.* **2019**, *727*, 19–24. [CrossRef]
79. Yeh, B.-Y.; Jian, B.-S.; Wang, G.-J.; Tseng, W.J. Cuo/v_2o_5 hybrid nanowires for highly sensitive and selective h2s gas sensor. *RSC Adv.* **2017**, *7*, 49605–49612. [CrossRef]

80. Wang, R.; Yang, S.; Deng, R.; Chen, W.; Liu, Y.; Zhang, H.; Zakharova, G.S. Enhanced gas sensing properties of v_2o_5 nanowires decorated with sno_2 nanoparticles to ethanol at room temperature. *RSC Adv.* **2015**, *5*, 41050–41058. [CrossRef]
81. Jin, W.; Dong, B.; Chen, W.; Zhao, C.; Mai, L.; Dai, Y. Synthesis and gas sensing properties of fe_2o_3 nanoparticles activated v_2o_5 nanotubes. *Sens. Actuators B Chem.* **2010**, *145*, 211–215. [CrossRef]
82. Avansi, W.; Catto, A.C.; da Silva, L.F.; Fiorido, T.; Bernardini, S.; Mastelaro, V.R.; Aguir, K.; Arenal, R. One-dimensional v_2o_5/tio_2 heterostructures for chemiresistive ozone sensors. *ACS Appl. Nano Mater.* **2019**, *2*, 4756–4764. [CrossRef]
83. Kim, J.-H.; Lee, J.-H.; Park, Y.; Kim, J.-Y.; Mirzaei, A.; Kim, H.W.; Kim, S.S. Toluene- and benzene-selective gas sensors based on pt- and pd-functionalized zno nanowires in self-heating mode. *Sens. Actuators B Chem.* **2019**, *294*, 78–88. [CrossRef]
84. Yang, X.; Wang, W.; Wang, C.; Xie, H.; Fu, H.; An, X.; Jiang, X.; Yu, A. Synthesis of au decorated v_2o_5 microflowers with enhanced sensing properties towards amines. *Powder Technol.* **2018**, *339*, 408–418. [CrossRef]
85. Sanger, A.; Kumar, A.; Kumar, A.; Jaiswal, J.; Chandra, R. A fast response/recovery of hydrophobic pd/v_2o_5 thin films for hydrogen gas sensing. *Sens. Actuators B Chem.* **2016**, *236*, 16–26. [CrossRef]
86. Suematsu, K.; Kodama, K.; Ma, N.; Yuasa, M.; Kida, T.; Shimanoe, K. Role of vanadium oxide and palladium multiple loading on the sensitivity and recovery kinetics of tin dioxide based gas sensors. *RSC Adv.* **2016**, *6*, 5169–5176. [CrossRef]
87. Mirzaei, A.; Kim, J.-H.; Kim, H.W.; Kim, S.S. Resistive-based gas sensors for detection of benzene, toluene and xylene (btx) gases: A review. *J. Mater. Chem. C* **2018**, *6*, 4342–4370. [CrossRef]
88. Feng, C.; Li, X.; Wang, C.; Sun, Y.; Zheng, J.; Lu, G. Facile synthesis benzene sensor based on v_2o_5-doped sno_2 nanofibers. *RSC Adv.* **2014**, *4*, 47549–47555. [CrossRef]
89. Mirzaei, A.; Janghorban, K.; Hashemi, B.; Neri, G. Metal-core@metal oxide-shell nanomaterials for gas-sensing applications: A review. *J. Nanopart. Res.* **2015**, *17*, 371. [CrossRef]
90. Mirzaei, A.; Kim, J.-H.; Kim, H.W.; Kim, S.S. How shell thickness can affect the gas sensing properties of nanostructured materials: Survey of literature. *Sens. Actuators B Chem.* **2018**, *258*, 270–294. [CrossRef]
91. Kim, J.-H.; Mirzaei, A.; Kim, H.W.; Kim, S.S. Low power-consumption co gas sensors based on au-functionalized sno_2-zno core-shell nanowires. *Sens. Actuators B Chem.* **2018**, *267*, 597–607. [CrossRef]
92. Shah, A.H.; Liu, Y.; Nguyen, V.T.; Zakharova, G.S.; Mehmood, I.; Chen, W. Enhanced ultra-stable n-propylamine sensing behavior of v_2o_5/in_2o_3 core–shell nanorods. *RSC Adv.* **2015**, *5*, 54412–54419. [CrossRef]
93. Mane, A.A.; Nikam, S.A.; Moholkar, A.V. No2 gas sensing properties of sprayed composite porous moo_3-v_2o_5 thin films. *Mater. Chem. Phys.* **2018**, *216*, 294–304. [CrossRef]
94. Mane, A.A.; Maldar, P.S.; Desai, S.P.; Moholkar, A.V. Gas sensing properties of $(moo_3)_{0.4}(v_2o_5)_{0.6}$ microsheets: Effect of pd sensitization. *Vacuum* **2017**, *144*, 135–144. [CrossRef]
95. Diniz, M.O.; Golin, A.F.; Santos, M.C.; Bianchi, R.F.; Guerra, E.M. Improving performance of polymer-based ammonia gas sensor using poma/v_2o_5 hybrid films. *Org. Electron.* **2019**, *67*, 215–221. [CrossRef]
96. Wang, J.; Wang, J.; Kong, Z.; Lv, K.; Teng, C.; Zhu, Y. Conducting-polymer-based materials for electrochemical energy conversion and storage. *Adv. Mater.* **2017**, *29*, 1703044. [CrossRef]
97. Zhang, J.; Ouyang, J.; Ye, Y.; Li, Z.; Lin, Q.; Chen, T.; Zhang, Z.; Xiang, S.J. Mixed-valence cobalt (ii/iii) metal–organic framework for ammonia sensing with naked-eye color switching. *ACS Appl. Mater. Interfaces* **2018**, *10*, 27465–27471. [CrossRef]
98. Naderi, H.; Hajati, S.; Ghaedi, M.; Dashtian, K.; Sabzehmeidani, M.M. Sensitive, selective and rapid ammonia-sensing by gold nanoparticle-sensitized v_2o_5/$cuwo_4$ heterojunctions for exhaled breath analysis. *Appl. Surf. Sci.* **2020**, *501*, 144270. [CrossRef]
99. Zhang, F.; Wang, X.; Dong, J.; Qin, N.; Xu, J. Selective btex sensor based on a sno_2/v_2o_5 composite. *Sens. Actuators B Chem.* **2013**, *186*, 126–131. [CrossRef]
100. Modafferi, V.; Trocino, S.; Donato, A.; Panzera, G.; Neri, G. Electrospun v_2o_5 composite fibers: Synthesis, characterization and ammonia sensing properties. *Thin Solid Film* **2013**, *548*, 689–694. [CrossRef]
101. Xiao, B.; Huang, H.; Yu, X.; Song, J.; Qu, J. Facile synthesis of layered v_2o_5/znv_2o_6 heterostructures with enhanced sensing performance. *Appl. Surf. Sci.* **2018**, *447*, 569–575. [CrossRef]

102. Wang, Y.; Zhou, Y.; Meng, C.; Gao, Z.; Cao, X.; Li, X.; Xu, L.; Zhu, W.; Peng, X.; Zhang, B.; et al. A high-response ethanol gas sensor based on one-dimensional tio_2/v_2o branched nanoheterostructures. *Nanotechnology* **2016**, *27*, 425503. [CrossRef] [PubMed]
103. Nagaraju, P.; Vijayakumar, Y.; Reddy, M.V.R.; Deshpande, U.P. Effect of vanadium pentoxide concentration in zno/v_2o_5 nanostructured composite thin films for toluene detection. *RSC Adv.* **2019**, *9*, 16515–16524. [CrossRef]